MAL-DISTRIBUTION MODEL OF HEAT EXCHANGERS IN MICRO CHANNEL EVAPORATOR

Santhosh Kumar
Student(M.Tech) , Mechanical Dept
Gokul group of institutions
Visakhapatnam, India

M Karteek Naidu
ASST PROFF, Mechanical Dept
Gokul group of institutions
Visakhapatnam, India

Abstract— This paper describes modeling and simulation of two phase mass flow distribution in a micro channel evaporator. primary pressure drop across the micro channel tube is the major drop considered and modeled. The global flow distribution is based on the mechanistic fact that the pressure drop along each flow path containing an individual micro channel tube must be the same. These include the frictional pressure loss along the inlet/outlet headers, as well as contraction and expansion loss associated with fluid entering and leaving the tube. Mass flow rate and quality in each microchannel tube, overall pressure drop and evaporator surface temperatures are calculated and then compared to data taken from the experimental facility. In order to compare cooling capacity prediction, the mass flow rate in the uniform distribution model was then increased until the exit superheat matched the superheat of the maldistribution model.

Keywords— Microchannel; kloss coefficient; Heat Exchangers.

I. INTRODUCTION

Microchannel evaporators typically have an advantage over conventional tube-fin heat exchangers in that they have high thermal performance for their size, and could have low capital cost. However, maldistribution of refrigerant among parallel channel tubes is a problem found in parallel microchannel heat exchangers that has various detrimental effects on performance. It causes certain tubes of the evaporator to receive more vapor phase refrigerant, which will create a large superheated zone and decrease local heat transfer rate, while other tubes have more liquid refrigerant which leaves in a two-phase state when flow is controlled by overall superheat. In order to satisfy the demand for the refrigerant to be superheated at the exit, the overall mass flow rate entering the evaporator must be reduced and the saturation temperature of the refrigerant must be lowered to create a larger temperature difference. Lowering the evaporation temperature causes a reduction in system COP. Many studies have been performed to understand how distribution of

refrigerant occurs, what it affects, and the way it is exacerbated.A few studies on the effects of maldistribution on system performance have been completed. Beaver, Yin, Bullard, and Hrnjak (1999) found that using a vapor-liquid separator prior to the evaporator improved distribution in the evaporator and thus caused better performance. Milosevic (2010) compared the use of a separator to a conventional vapor-compression system and found the improvement in distribution caused up to a 55% increase in overall system COP. The evaporator in that study was relatively undersized, which was the cause of the large performance increase. A study by Tuo, Bielskus, and Hrnjak (2011) showed performance gains of 11% and 16% for COP and cooling capacity, respectively and simultaneously, when using a flash gas separator to improve distribution.

II. EXPERIMENTAL FACILITY

The experiment section was conducted on a standard mobile air conditioning system. The system is described in detail by Milosevic (2010). In the system, there is an outdoor and indoor chamber separated from the compressor. Each chamber contains a wind tunnel where the evaporator or condenser resides, as well as a variable speed blower and duct heater. In the condensing chamber, the heat rejected from the system is removed through the use of a heat exchanger supplied with external coolant from a chiller. There is a duct heater in either chamber controlled by a PID controller. The duct heater in the evaporating chamber supplies heat equivalent to the heat added into the system. The duct heater in the condensing chamber is there to more effectively control the temperature of the condensing chamber, rather than relying explicitly on the mass flow and temperature of the glycol loop. There are three ways to calculate heat rejected or added into the system: Chamber side, air side, and refrigerant side. The schematic of the system is presented below:
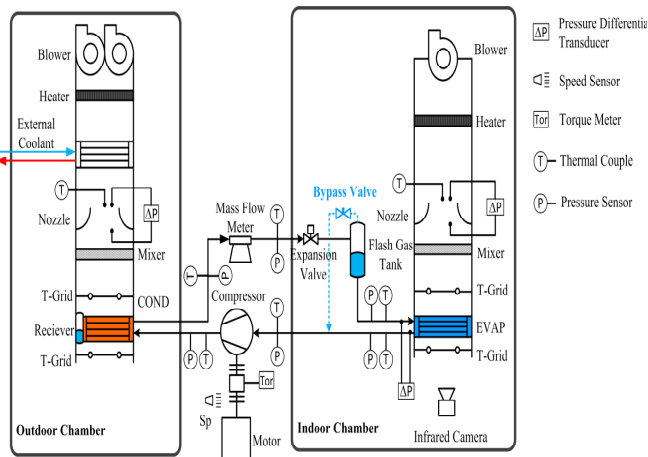
Figure 2.1: Experimental facility schematic

In figure 2.1 in the indoor chamber, there is a flash gas tank with a bypass valve connecting the tank to the suction line of the compressor. The bypass valve is a standard needle valve that can be opened and closed. If the bypass valve is closed, the system operates as a typical vapor compression system, and the flash tank has no effect. This mode is referred to as Direct Expansion (DX) mode. When the bypass valve is opened, the flash gas is separated from the liquid in the flash gas tank and bypassed over the evaporator. This is referred to as the flash gas bypass (FGB) configuration. Thus, two distinct flow conditions at the evaporator inlet are provided. For DX operation, two phase refrigerant enters the evaporator, and the flow rate is measured by a flow meter installed before the electronic expansion valve. For FGB operation, only saturated refrigerant with a quality of zero enters the evaporator; in this case, flow rate is determined by adjusting the measured flow rate from mass flow meter by the quality calculated at the inlet of the flash gas tank.

Data is acquired into the system using a Hewlett-Packard data acquisition system HP75000. HP VEE 6.0 software is used to acquire the data and record it to a Microsoft Excel data sheet. The data is then copied from the Excel data sheet and placed into an EES program. The EES program reduces all the data and calculates results such as system COP, cooling capacity, pressure drop, and other data. The following heat exchanger was used in the experiment and simulated in the model.

This heat exchanger allowed connections on either side of both headers. The heat exchanger was connected to the system in two ways: with the inlet and outlet on the opposite side and inlet and outlet on the same side. Figures 2.3 and 2.4 illustrate this in greater detail. The location of pressure measurements is also shown, with the pressure transducers represented as circles. The values that are boxed indicate pressures calculated by the model.
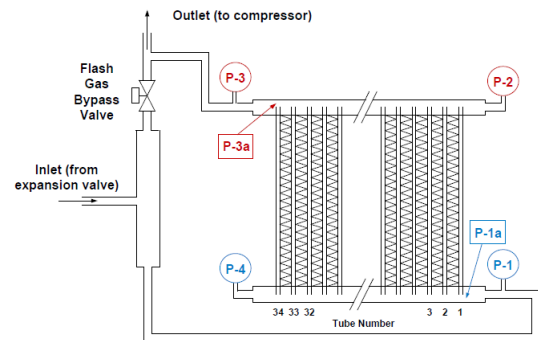

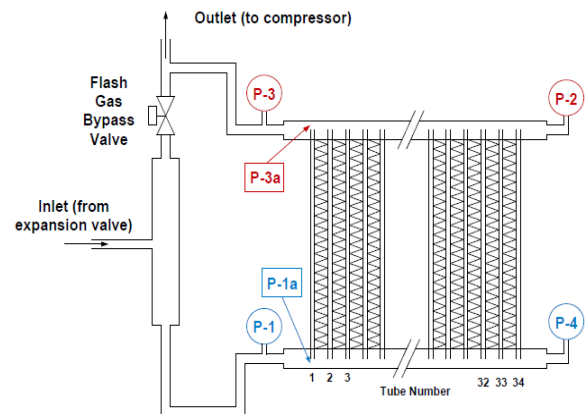**Figure 2.3: Microchannel evaporator in opposite side configuration**

Figure 2.4: Microchannel Evaporator in same side configuration

Table 2.1: Microchannel evaporator specifications

| Heat Exchanger Physical Parameters	
Face Area (m^2)	0.068
Fin Pitch (mm)	1.3
Fin Height (mm)	7.9
Fin Depth (mm)	21.3
Fin Thickness (mm)	.1
Louver angle (deg)	27
Louver pitch (mm)	1.4
Louver Height (mm)	6.6
Air heat Transfer Area (m^2)	0.0825
Tube Number	34
Tube Pitch (mm)	9.8
Tube Depth (mm)	18.8
Tube Length (mm)	275
Tube Thickness (mm)	1.9
Number of ports per tube (mm)	19
Hydraulic Diameter (mm)	.77
Refrigerant Heat Transfer Area (m^2)	.019
Header Diameter (mm)	20.3
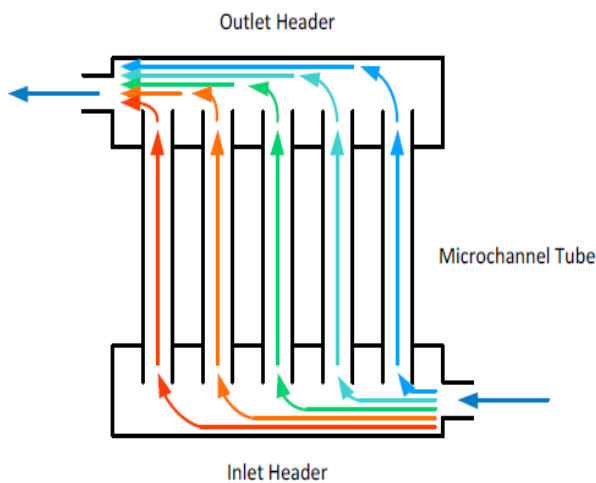
Figure 3.1: Flow path description

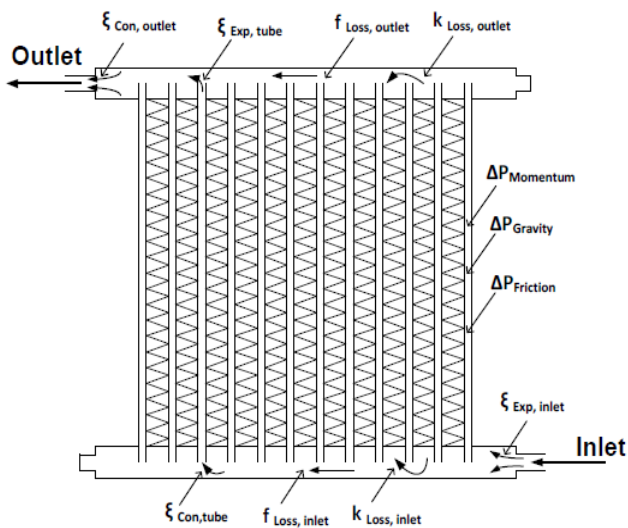The pressure drops that are taken into account in the EES model are illustrated below:

Figure 3.2: Characterized pressure drops in the model

IV. RESULTS

Overall pressure drop, cooling capacity, and superheat at the exit of the evaporator from the experimental results are used to validate the model. The inputs given to the model from experimental data consist of total mass flow rate, the inlet quality to the separator (FGB Case) or to the evaporator (DX Case), refrigerant inlet saturation temperature, air inlet temperature, and air flow rate.

4.1 Kloss Determination

Before validation can be done, the kloss coefficient in the headers, defined in equation 3-43, must be chosen according to the experimental data. The minor pressure loss through the headers and its order of magnitude in relation to the microchannel tube pressure drop is what determines the deviation in refrigerant distribution. The pressure drop through the header is

largely caused by the 50% protrusion of the microchannel tubes into the inlet and outlet headers. There has not been any study or related correlation predicting this minor loss completed in open literature. The closest work was performed by Yin et. al (2002). His work was on characterization of pressure drops in a parallel microchannel

heat exchanger with adiabatic single phase nitrogen. Yin supplied nitrogen only through the inlet header and measured the pressure drop across the header, and then calculated the kloss coefficient from the results. He found that over a Reynold's number range of ~100 to ~100000, the kloss calculation is around 0.4 for that particular heat exchanger header size, with some variance in the measurement around low Reynold's numbers. Because of the very wide range of Reynold's numbers and thus mass fluxes, the kloss can be assumed to be constant across the entire range of mass flow rates. Unfortunately, Yin did not provide a correlation to predict the kloss coefficient if the header geometric properties are known. Thus, one must be determined using experimental data.

Table 4.1: Pressure drop, cooling capacity, and superheat predictions for various kloss coefficients

K loss	Overall ΔP	% Diff	ΔP (1-2)	% Diff	ΔP (2-4)	% Diff	ΔP (3-4)	% Diff	Q (kW)	% Diff	Superheat (°C)	Δ°C
Exp Data	16.4		2.7		1.4		15.0		3.3		14.0	
0.7	16.4	-0.1	2.6	4.7	2.3	-69.8	16.2	-8.1	3.3	-0.7	14.3	0.3
0.75	16.6	-1.2	2.4	9.8	2.2	-58.2	16.4	-9.3	3.3	0.0	12.8	-1.2
0.85	17.0	-3.7	2.3	14.5	2.0	-45.8	16.7	-11.7	3.2	1.5	9.3	-4.7
0.95	17.5	-6.2	2.2	18.6	1.9	-34.7	17.1	-14.2	3.2	2.9	6.4	-7.5
1.05	17.8	-8.5	2.1	22.5	1.7	-23.8	17.4	-16.4	3.2	4.2	3.5	-10.5
1.15	18.2	-10.8	2.0	26.3	1.6	-16.1	17.7	-18.2	3.1	5.8	0.8	-13.2
1.25	18.5	-12.6	1.9	30.0	1.4	-1.6	18.0	-20.2	3.1	6.7	0.0	-14.0

4.2 Opposite Side Configuration – Flash Gas Bypass

The following data table presents the measured vs. the predicted values run for the entire range of test conditions for the opposite side – FGB case. "Opposite side configuration" refers to the orientation of the inlet and outlet connections to the headers, illustrated in figure 2.3.

Table 4.2: Experimentally measured vs. predicted values for opposite side – fgb configuration

Mass Flow Rate (g/s)	Evaporator Ref. Inlet Temperature (°C)	Evaporator Air Inlet Temperature (°C)	Overall ΔP - Measured (kPa)	Overall ΔP - Predicted (kPa)	Q - Measured (kW)	Q - Predicted (kW)	Superheat - Measured (°C)	Superheat - Predicted (°C)
7.0	3.7	25.7	5.2	4.1	1.5	1.5	19.9	21.0
8.6	6.9	25.5	6.3	5.7	1.8	1.8	14.5	17.2
9.8	9.0	25.1	7.2	7.0	1.9	2.0	7.4	11.7
10.5	10.4	25.9	7.6	7.6	2.1	2.0	0.6	5.1
14.7	6.0	35.6	14.9	14.6	3.1	3.2	20.7	25.0
16.2	7.7	35.6	16.4	16.4	3.3	3.3	14.0	14.3
17.2	8.7	35.5	17.6	17.6	3.4	3.4	3.5	4.6
18.0	9.4	35.6	18.1	18.4	3.5	3.4	0.0	0.0
17.8	5.3	40.6	21.7	20.9	3.7	3.8	21.2	24.8
19.3	7.0	40.6	23.2	22.7	4.0	3.9	14.6	13.7
19.9	7.6	40.5	23.7	23.4	4.0	4.0	7.3	7.9
20.2	8.0	40.6	24.2	23.6	4.0	4.0	4.8	5.5

The prediction for the overall pressure drop, cooling capacity, and superheat appears to be fairly good. The most important prediction of all of these values is the superheat prediction, which separates the mass flow rate distribution model from the uniform distribution model, which assumes that refrigerant is equally distributed among parallel tubes. The following mass flow rate profile represents the 16.2 g/s mass flow rate case from table 4.2. The superheat at each tube number represents the superheat at the exit of the tubes.
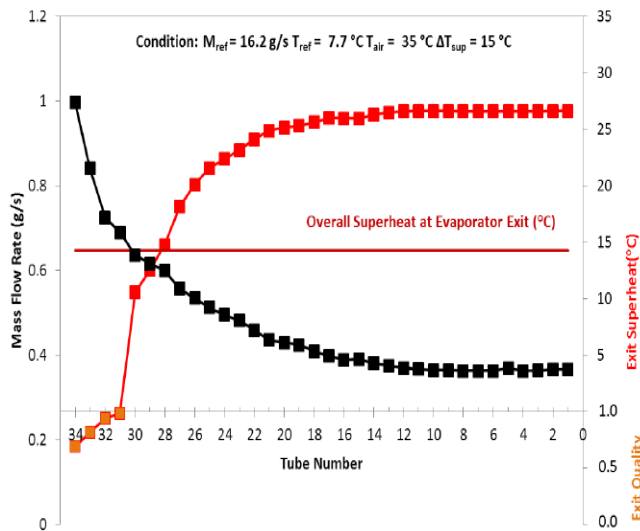

Figure 4.1: Mass flow rate and exit superheat distribution among the tubes, and average superheat at evaporator exit for FGB operation, opposite side configuration

Another method to verify the mass flow rate profile prediction and thus the superheat prediction is to compare the wall temperature profile taken by infrared camera to the wall temperatures predicted by the model. Unfortunately, the mass flow rate prediction cannot be directly validated through this method. The mass flow rate in each microchannel

tube cannot be measured in an evaporator working in a standard air conditioning system without using an intrusive method, thereby altering the physical phenomena occurring. However, the evaporator surface temperature profile can indicate the mass flow rate distribution indirectly.
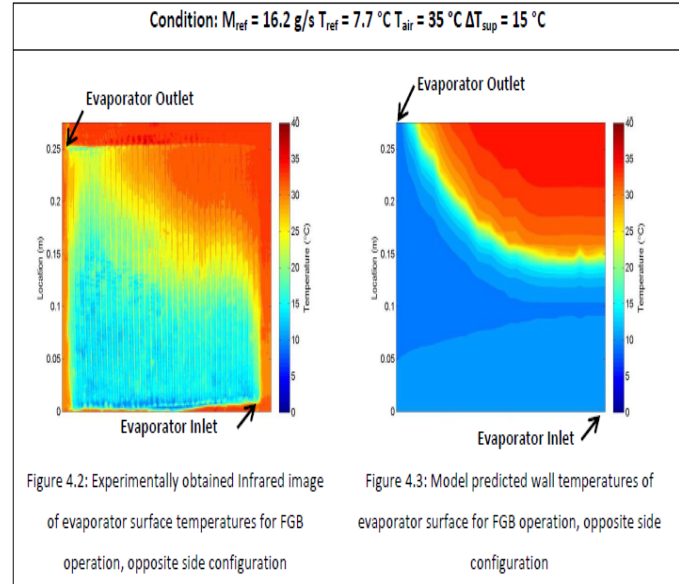

Figure 4.2: Experimentally obtained Infrared image of evaporator surface temperatures for FGB operation, opposite side configuration

Figure 4.3: Model predicted wall temperatures of evaporator surface for FGB operation, opposite side configuration

Both the experimental and model predicted superheat profiles are similar, in that the tubes on the far left in figure 4.2 appear to have refrigerant that is two-phase at the exit.

CONCLUSION

The model developed satisfactoraly predicts cooling capacity, pressure drop, and exit superheat. Compared with the uniform distribution model, the superheat is consistently better predicted. The model uses the kloss coefficient determined through experimental results for the opposite side FGB case. The sensitivity of the model to the kloaa coefficient was conducted, and the kloss of 0.7 was determined based on good confirmation of experimental results. Developing a correlation for kloss based on header geometric parameters would allow the model to be used in a predictive fashion, rather than confirming experimental results. Work is being continued on the kloss coefficient determination. The superheat in the DX case is consistently overpredicted when the inlet and outlet are on opposite sides of the evaporator. This may be due to incorrect characterization of the inlet header pressure drop, which is increased over the FGB case due to the significantly higher density. Development of a two-phase pressure drop correlation for the inlet header pressure drop that is underway will improve the fidelity and generality of the model. Using the uniform distribution model gives

acceptable accuracy in predicting superheat only in the case where all of the parallel tubes are superheated at their exits. This only occurred in the 25 °C data set for the two low flow rates, limiting the robustness of the uniform distribution model. As the superheat decreases, the error in superheat prediction of the uniform distribution model increases. When the inlet mass flow rate of the evaporator is composed of saturated liquid, mass flow rate distribution is driven solely by the magnitude of microchannel tube pressure drop in relation to the magnitude of pressure drop through the inlet and outlet headers, respectively. In this case, maldistribution can be eliminated by decreasing the relative magnitude of the header pressure drops.

REFERENCES

[1]   Ablanque, N. N., Oliet, C. C., Rigola, J. J., Pérez-Segarra, C. D., & Oliva, A. A. (2010). Two-phase flow distribution in multiple parallel tubes. International Journal of Thermal Sciences, 49(6), 909-921.

[2]   Beaver, A.C., Yin, J.M., Bullard, C.W., & Hrnjak, P.S., (1999). An Experimental Investigation of Transcritical Carbon Dioxide Systems for Residential Air Conditioning. Contract Report CR-18, Air Conditioning and Refrigeration Center, University of Illinois, Urbana-Champaign, IL.

[3]   Bowers, C.D., Newell, T.A., & Hrnjak, P.S. (2006). Experimental Investigation of Two-Phase Refrigerant Distribution in a Microchannel Manifold. Technical Report TR-245, Air Conditioning and Refrigeration Center, University of Illinois, Urbana-Champaign, IL.

[4]   Bowers, C.D., & Hrnjak, P.S. (2009). Developing Adiabatic Two-Phase Flow. Technical Report TR-267, Air Conditioning and Refrigeration Center, University of Illinois, Urbana-Champaign, IL.

[5]   Brix, W., Kærn, M., & Elmegaard, B. (2009). Modelling refrigerant distribution in microchannel evaporators. International Journal of Refrigeration, 32(7), 1736-1743.

[6]   Brix, W., Kærn, M., & Elmegaard, B. (2010). Modelling distribution of evaporating CO_2 in parallel minichannels. International Journal of Refrigeration, 33(6), 1086-1094.

[7]   Chen, J. C., (1966). Correlation for boiling heat transfer to saturated fluids in convective flow. Ind. Eng. Chem. Proc. Design and Dev., 5(3), 322-339.

[8]   Churchill, S. W. (1977). Friction factor equation spans all fluid-flow regimes. Chemical Engineering, 84(24), 91-92.

[9]   Fei, P., Cantrak, Dj., & Hrnjak, P.S., (2002). Refrigerant Distribution in the Inlet Header of Plate Evaporators, 2002 SAE World Congress, Paper # 2002-01-0948.

[10]   Forster, H. K., & Zuber, N. (1955). Dynamics of vapor bubbles and boiling heat transfer. AIChE Journal, 1, 531-535.

[11]   Friedel, L. (1979). Improved friction pressure drop correlations for horizontal and vertical two-phase pipe flow. Paper E2, European Two Phase Flow Group Meeting, Ispra, Italy.

[12]   Gnielinski, V. (1976). New Equations for Heat and Mass Transfer in Turbulent Pipe and Channel Flow. International Chemical Engineering,16(2), 359-368.

[13]   Hwang, Y., Jin, D.H., & Radermacher, R. (2007). Refrigerant Distribution in Minichannel Evaporator Manifolds. HVAC&R Research, 13, Number 4, 543-555.